Reaction Kinetics, Mechanisms and Catalysis (2020) 130:825–836
https://doi.org/10.1007/s11144-020-01799-4

Role of Brønsted and Lewis acidic sites in sulfonated Zr-MCM-41 for the catalytic reaction of cellulose into 5-hydroxymethyl furfural

Son Tung Pham[1,2] · Ba Manh Nguyen[1] · Giang H. Le[1] · Andras Sapi[3,4] · Suresh Mutyala[3] · Imre Szenti[3,5] · Zoltan Konya[3,5] · Tuan A. Vu[1]

Received: 7 March 2020 / Accepted: 7 June 2020 / Published online: 1 July 2020

Abstract

A series of sulfonated Zr-MCM-41 samples were synthesized by the in-situ method followed by sulfonation using sulfuric acid for the catalytic study of cellulose to 5-hydroxymethyl furfural in batch condition. All synthesized catalysts were characterized by XRD, N_2 adsorption–desorption isotherm, FT-IR, TEM, EDX, and NH_3 temperature-programmed desorption analysis. The XRD and N_2 adsorption–desorption isotherm results have confirmed that incorporated Zr^{4+} was substituted within the framework of silica MCM-41 with hexagonal pores. Similarly, the FT-IR and EDX results have proved that Zr-MCM-41 was sulfonated. The Brønsted acidic and Lewis acidic sites were identified by NH_3-TPD analysis. Among the sulfonated Zr-MCM-41 catalysts, S-15Zr-MCM-41 has shown 70% cellulose conversion with 16.4% selectivity of 5-hydroxymethyl furfural at 170 °C for 2 h which was higher than other catalysts. It was attributed to the high ratio of Brønsted acidic to Lewis acidic sites.

✉ Andras Sapi
sapia@chem.u-szeged.hu

[1] Institute of Chemistry, Vietnam Academy of Science and Technology (VAST), Hanoi, Vietnam

[2] Vietnam National University (VNU), Hanoi, Vietnam

[3] Interdisciplinary Excellence Centre, Department of Applied and Environmental Chemistry, University of Szeged, Rerrich Bela ter 1, 6720 Szeged, Hungary

[4] University of Szeged, Institute of Environmental and Engineering Sciences, Rerrich Bela ter 1, 6720 Szeged, Hungary

[5] MTA-SZTE Reaction Kinetics and Surface Chemistry Research Group, University of Szeged, Rerrich Bela ter 1, 6720 Szeged, Hungary

Graphic abstract

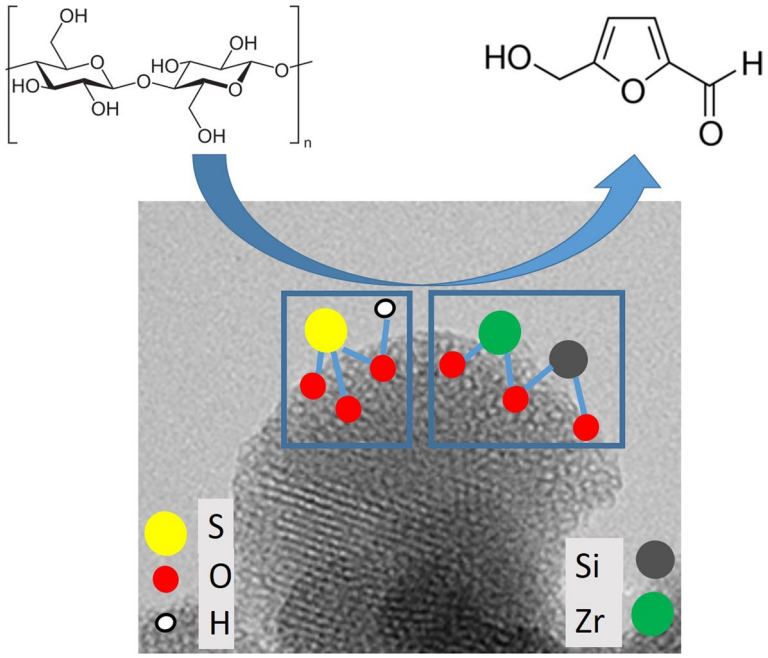

Keywords Zr-MCM-41 · Sulfonation · Brønsted & lewis acidity · Cellulose · 5-HMF

Introduction

5-Hydroxymethyl furfural (5-HMF) is a major important platform chemical that could be produced from cellulose and hemicellulose by hydrolysis in the acidic medium [1–3]. It is an intermediate in biomass-based carbohydrate chemistry and petroleum-based industrial chemistry to produce chemicals and fuels [4, 5]. Production of 5-HMF from cellulose involved 3 steps catalytic mechanism: hydrolysis of cellulose to glucose by Brønsted acid, isomerization of glucose to fructose by Lewis acid assistance, and dehydration of fructose to 5-HMF by Brønsted acid [6]. Few research groups have studied the conversion of cellulose to 5-HMF using homogeneous catalysts such as H_2SO_4, HCl-$AlCl_3$, $CrCl_2$-$CrCl_3$, $ZrOCl_2$/$CrCl_3$ [7–11]. However, they have reported some issues such as lack of separation of the catalyst, corrosion, and toxicity. These can be overcome by the use of solid acid catalyst [12–17].

As mentioned above, the conversion of cellulose to 5-HMF is catalyzed by Brønsted acidic and Lewis acidic sites. For this purpose, bifunctional solid acid catalysts have been developed and used. Mazzotta et al. have reported the effectiveness of Ti(IV)-HSO_3 catalyst for the dehydration of cellulose, glucose, and fructose. They

depicted the dual role of Brønsted acidic and Lewis acidic sites for biomass conversion [18]. Similarly, Osatiashtiani et al. have used bifunctional sulfonated zirconia (S-ZrO_2) catalyst for the conversion of glucose to 5-HMF [6]. The effectiveness of this catalyst was increased by impregnation on mesoporous silica, SBA-15 [19]. Mesoporous silica materials like SBA-15 and MCM-41 have been widely used as support due to high surface area 600–1200 m^2/g and tunable pore size 2–50 nm [20–22].

Based on the above concept, in this article, we have studied the catalytic reaction of cellulose to 5-HMF in a batch reactor using sulfonated Zr-MCM-41 catalysts synthesized by in-situ method followed by sulfonation. Moreover, the role of Brønsted acidic and Lewis acidic sites presented in the synthesized catalyst useful for the catalytic reaction was also discussed.

Experimental

Materials

Analytical grade chemicals like zirconium (IV) sulfate ($Zr(SO_4)_2$), Tetraethyl orthosilicate ($SiC_8H_{20}O_4$, TEOS), ammonium hydroxide (NH_5O, 25wt%), cetyltrimethylammonium bromide ($C_{19}H_{42}BrN$, CTABr), sulfuric acid (H_2SO_4), cellulose ($(C_6H_{10}O_5)_n$) and 5-hydroxy methyl furfural ($C_6H_6O_3$) were purchased from the M/s. Sigma Aldrich Chemicals Pvt. Ltd., Vietnam, and used without purification.

Synthesis of MCM-41 and sulfonated Zr-MCM-41

MCM-41 was synthesized by the soft template method using CTABr as a template. The desired quantities of TEOS, CTABr, and NH_4OH were mixed in a glass beaker until a homogeneous solution was obtained. The mixture was transferred into a Teflon lined autoclave and kept at 100 °C for 24 h. A white precipitate was formed. It was filtered and washed with distilled water then dried at 100 °C for 12 h. Finally, it was calcined at 550 °C for 4 h in static air. We obtained MCM-41 [23]. Zr-MCM-41 was synthesized using the same procedure as that of MCM-41 with Zr/Si ratio (4, 8, 12, 15, 20 wteqauti%). To sulfonate Zr-MCM-41, it was treated with 1 M H_2SO_4 at room temperature for 1 h followed by filtration and washed with distilled water then dried at 100 °C for 12 h. We obtained sulfonated Zr-MCM-41 and labeled as S-xZr-MCM-41, where x represents the wt% of Zr loaded.

Characterization

The X-ray diffractions were recorded using a D8 Advance X-ray diffractometer having Ni filtered Cu K_α radiation in the range from $2\theta = 0.7–70°$ with a scan speed of 2°/min. The N_2 adsorption–desorption isotherms were measured using Micromeritics Tristar 3000 gas adsorption analyzer at 77 K. Before the isotherm measurement, 0.1 g of sample was activated at 200 °C for 3 h under vacuum to remove

moisture. The surface area was calculated by the multipoint BET method, total pore volume at $P/P_0 = 0.99$, and pore size by the BJH method. TEM images were recorded using FEI TECNAI G2 20 X-Twin high-resolution transmission electron microscopy operated at high voltage 200 kV. Energy-dispersive X-ray spectroscopy analysis was performed using Hitachi S-4700 scanning electron microscopy. FT-IR spectra were recorded on the JASCO FT-IR-4100 spectrometer in the range from 4000 – 400 cm^{-1} with a resolution of 4 cm^{-1} using the KBr disc method. Ammonia temperature-programmed desorption (NH_3-TPD) was measured using Micromeritics Autochem-II 2920 analyzer from 100–600 °C with a heating rate of 10°/min.

Catalytic study of S-Zr-MCM-41

The catalytic reaction of cellulose to 5-HMF using S-Zr-MCM-41 catalysts was carried out in a Teflon-lined stainless steel reactor equipped with a mechanical stirring system. The reaction mixture, 2 g cellulose, 0.2 g catalyst, and 10 mL water were transferred into 50 mL reactor then the temperature was raised to 170 °C with a heating rate of 10 °C/min and kept at this temperature for 2 h with a rotation speed of 400 rpm/min. The reaction products were collected by centrifugation and analyzed using GC–MS Agilent 7890A with MS detector.

Results and discussion

X-ray diffraction analysis

The low and wide-angle XRD patterns of MCM-41 and sulfonated Zr-MCM-41 were shown in Fig. 1. MCM-41 has shown 3 peaks at $2\theta = 2°$, 3.7° and 4.4° with reflections planes (100), (110) and (200) respectively (JCPDS No. 00-049-1712) which were the main characteristic peaks of hexagonal mesoporous MCM-41 with a space group *P6mm* (Fig. 1a) [24]. Zr-MCM-41 catalysts have also shown

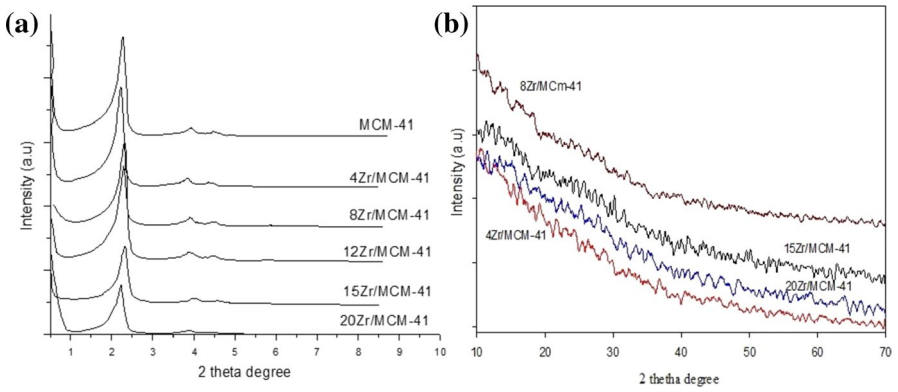

Fig. 1 XRD of MCM-41 and sulfonated Zr-MCM-41: **a** low angle and **b** wide-angle

a low angle XRD pattern similar to bulk MCM-41. However, a decrease in the intensity of major peaks has been observed with an increase in the amount of Zr. In wide-angle XRD of MCM-41 and Zr-MCM-41 samples, no diffraction peaks have appeared (Fig. 1b) [25]. The lattice parameters d_{100} and a_0 for all synthesized samples were presented in Table 1. The d-spacing (d_{100}) and unit cell parameter constant (a_0) were higher for higher loadings of Zr (12, 15, and 20 wt%) compared with bare MCM-41 because of the replacement of Si^{4+} by Zr^{4+} in the framework. Consequently, a change in lattice parameters has been observed.

N_2 adsorption–desorption isotherms

The N_2 adsorption–desorption isotherms of MCM-41 and sulfonated Zr-MCM-41 at 77 K were shown in Fig. 2 and textural properties were presented in Table 1. For MCM-41, a hysteresis loop has been observed above the relative pressure $P/P_0 = 0.85$ [26]. The isotherm curve of MCM-41 was similar to Type-IV with the H1 hysteresis loop of classification of the porous materials by IUPAC [27]. Therefore, it has mesopores. For sulfonated Zr-MCM-41 samples, a hysteresis loop has not appeared. It was due to the shrinkage of pore size by sulfonation. The calculated specific surface area, pore-volume, and pores size of MCM-41 was 1191 m^2/g, 1.99 cm^3/g, and 6.1 nm respectively. MCM-41 and S-4Zr-MCM-41 have shown surface area nearly the same. Further increase in Zr content, a change in textural properties has been observed. The surface area was reached to 874 m^2/g, pore volume 0.74 cm^3/g and pore size 3.6 nm. It was due to deformation effect of Zr ions incorporated into the structure of MCM-41.

Table 1 The lattice parameters and textural properties of MCM-41 and sulfonated Zr-MCM-41

Sample	d_{100}[a] (nm)	a_0[b] (nm)	S_{BET}[c] (m^2/g)	$S_{mesopore}$[d] (m^2/g)	V_{total}[e] (cm^3/g)	Pore size[f] (nm)
MCM-41	3.92	4.53	1191	826	1.99	6.1
S-4Zr-MCM-41	3.93	4.53	1243	825	1.27	3.7
S-8Zr-MCM-41	3.94	4.55	1040	664	0.91	3.5
S-12Zr-MCM-41	4.27	4.94	913	601	0.85	3.6
S-15Zr-MCM-41	4.34	5.01	1022	591	0.75	3.1
S-20Zr-MCM-41	4.23	4.89	874	575	0.74	3.6

[a]d-spacing at (100)

[b]unit cell parameter ($a_0 = 2d_{100}/\sqrt{3}$)

[c]BET surface area

[d]mesopore surface area

[e]total pore volume

[f]pore size by BJH method

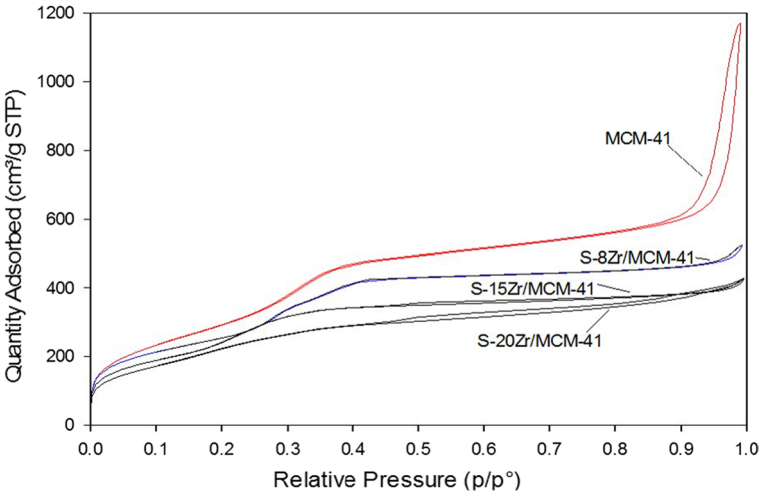

Fig. 2 N_2 adsorption–desorption isotherms of MCM-41 and sulfonated Zr-MCM-41

FT-IR analysis

FT-IR spectra of MCM-41 and sulfonated Zr-MCM-41 catalysts were shown in Fig. 3. For MCM-41, the bands appeared at 3450 cm^{-1} and 1640 cm^{-1} represented the stretching and bending vibrational bands of the O–H group of water. The symmetric and asymmetric vibrational bands of the Si–O-Si group have

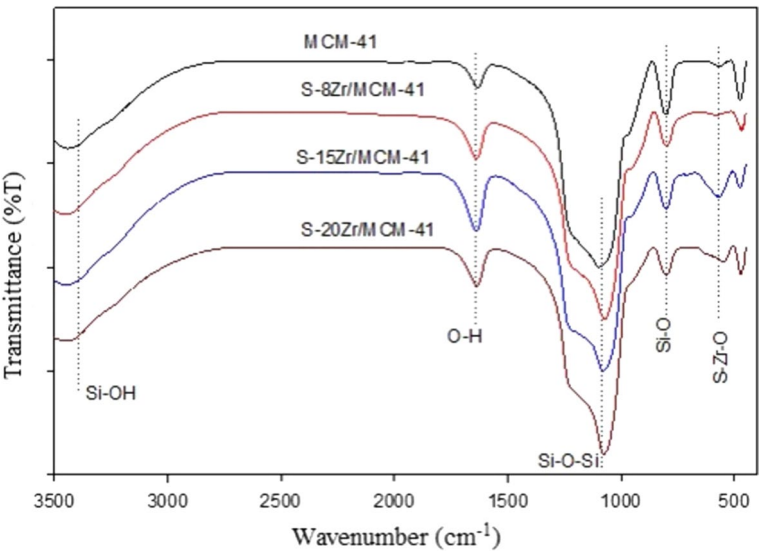

Fig. 3 FT-IR spectra of MCM-41 and S-Zr-MCM-41 samples

appeared at 1084 cm^{-1} and 826 cm^{-1} respectively. Moreover, the band appeared at 465 cm^{-1} represented the bending vibrational band of Si–O-Si (or) Zr–O–Si [25, 28]. In sulfonated Zr-MCM-41 samples, the major vibrational bands of MCM-41 have been replicated. Along with this, the SO_2 deformation band also appeared at 550 cm^{-1} [29]. Hence, FT-IR analysis has confirmed that the sulfonate group has been attached to the walls of Zr-MCM-41.

TEM and EDX analysis

Fig. 4 shows the TEM images of MCM-41 and sulfonated Zr-MCM-41. Ordered hexagonal pores were obtained for MCM-41 (Fig. 4a). For sulfonated Zr-MCM-41 samples, the same hexagonal pore structure was obtained. However, the particles correspond to zirconium oxide have not appeared. It confirmed that the incorporated zirconium was interconnected with the framework of MCM-41. The TEM analysis result was correlated with XRD. The content of zirconium in sulfonated Zr-MCM-41 samples was determined using energy-dispersive X-ray spectroscopy. Table 2 shows the elemental composition of sulfonated Zr-MCM-41 samples. Experimentally obtained Zr (wt%) was near to theoretically loaded amount. The amount of Sulphur in each sample was 10–12.5 wt%. It was also confirmed the presence of sulfur in the sulfonated Zr-MCM-41 samples.

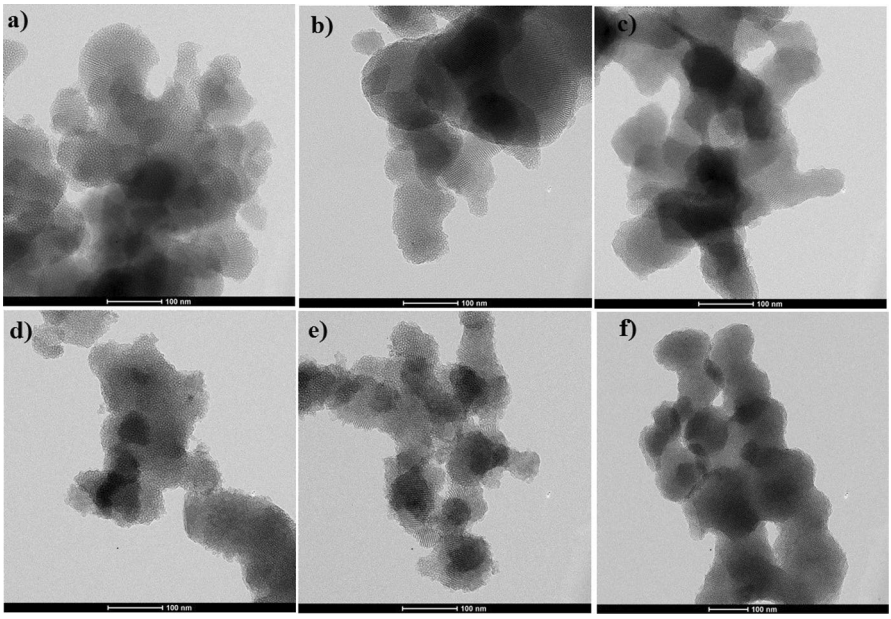

Fig. 4 TEM images of **a** MCM-41, **b** S-4Zr-MCM-41, **c** S-8Zr-MCM-41, **d** S-12Zr-MCM-41, **e** S-15Zr-MCM-41, and **f** S-20Zr-MCM-41 (scale bar- 100 nm)

Table 2 Elemental composition of sulfonated Zr-MCM-41 samples from EDX

Sample	Elements		
	Silicon (wt%)	Zirconium (wt%)	Sulphur (wt%)
S-4Zr-MCM-41	85.95	3.84	10.21
S-8Zr-MCM-41	81.27	7.23	11.50
S-12Zr-MCM-41	77.73	10.02	12.25
S-15Zr-MCM-41	73.44	14.78	11.78
S-20Zr-MCM-41	69.54	16.78	10.68

Temperature programmed desorption of NH_3

Ammonia temperature-programmed desorption profile of S-8Zr-MCM-41, S-15Zr-MCM-41, and S-20Zr-MCM-41 was shown in Fig. 5. The amount of NH_3 desorbed was presented in Table 3. Each sample has shown 3 desorption peaks in between the temperatures 140–170 °C, 250–270 °C and 470–570 °C which correspond to physisorbed ammonia, Brønsted acidic and Lewis acidic sites respectively [30]. By substitution of Si^{4+} by Zr^{4+} created Lewis acidic sites whereas sulfonated Zr-MCM-41 sample has generated Brønsted acidic sites (SO_3H^-). The total amount of NH_3 desorbed was 1.807 mmol/g for S-8Zr-MCM-41, 1.809 mmol/g for S-15Zr-MCM-41, and 1.259 mmol/g for S-20Zr-MCM-41. The catalyst S-8Zr-MCM-41 has shown high Lewis acidic sites whereas S-15Zr-MCM-41 has shown high Brønsted acidic sites. The order of the ratio of Brønsted acidic site to Lewis acidic site was S-15Zr-MCM-41 > S-8Zr-MCM-41 > S-20Zr-MCM-41. The synergetic of the skeleton

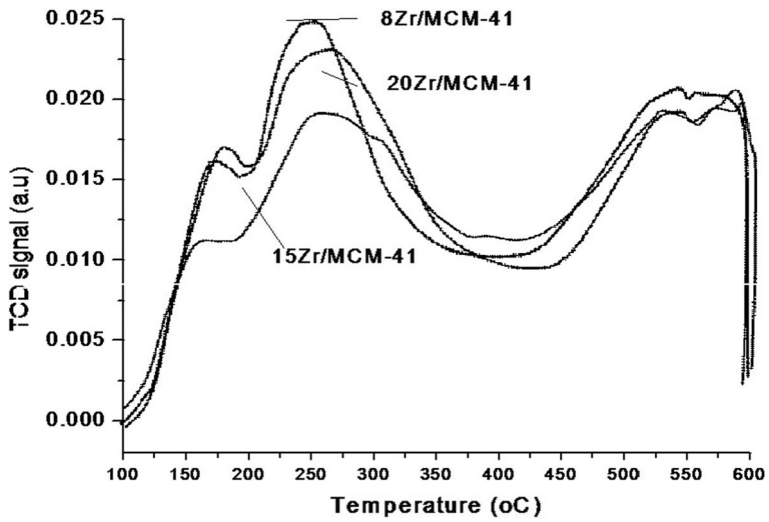

Fig. 5 NH_3 temperature-programmed desorption of S-Zr-MCM-41 samples

Table 3 Amount of NH_3 desorbed for S-Zr-MCM-41 samples

Sample	NH_3 desorbed (mmol/g)			Total NH_3 desorbed (mmol/g)	Ratio of B/L[a]
	T_{max} 140–170 °C	T_{max} 250–270 °C	T_{max} 470–570 °C		
S-8Zr-MCM-41	0.415	0.799	0.593	1.807	1.347
S-15Zr-MCM-41	0.404	0.986	0.419	1.809	2.353
S-20Zr-MCM-41	0.385	0.490	0.384	1.259	1.276

[a]Ratio of Bronsted acidic/Lewis acidic sites

structure, Zr loading and Sulphur surface concentration lead to variation in the type of acidic site strength.

Catalytic conversion of cellulose to 5-HMF

MCM-41 and sulfonated Zr-MCM-41 catalysts have been used for the catalytic conversion of cellulose to 5-HMF in the Teflon lined stainless steel reactor. The results were presented in Table 4. The conversion of cellulose without catalyst was 1.3% at 170 °C for 2 h. For MCM-41, the conversion was increased to 15.2% and S-Zr-MCM-41 catalysts 63.3–70.2%. The selectivity and yield of 5-HMF were higher with the increase in the amount of Zr. Yayati et al. have studied silica-supported tin catalyst for the catalytic reaction of glucose. It has converted glucose into fructose by isomerization because of the Lewis acidic nature of the catalyst [31]. In this article, the synthesized catalyst sulfonated Zr-MCM-41 has both Brønsted acidic and Lewis acidic sites. So, it converted cellulose into 5-HMF. Among the synthesized sulfonated Zr-MCM-41 catalysts, high conversion of cellulose and 5-HMF selectivity was obtained for S-15Zr-MCM-41 because of the high ratio of Brønsted acidic to Lewis acidic sites (NH_3-TPD analysis). Therefore, the catalyst which has Brønsted acidic and Lewis acidic properties are useful for the hydrolysis of cellulose and

Table 4 Catalytic reaction of cellulose to 5-hydroxymethyl furfural at 170 °C for 2 h

Catalyst	Conversion of cellulose (%)	Selectivity of 5-HMF (%)	Yield of 5-HMF (%)
No catalyst	1.3	0.8	0.01
MCM-41	15.2	1.3	0.2
S-4Zr-MCM-41	63.3	3.0	1.9
S-8Zr-MCM-41	64.5	10.6	6.8
S-12Zr-MCM-41	69.5	11.4	9.0
S-15Zr-MCM-41	70.2	16.4	11.5
S-20Zr-MCM-41	68.6	9.4	6.4

cellulose derivatives. In the forthcoming article, we want to study the optimization of catalyst quantity, temperature, reaction time, and recyclability.

Conclusion

In this work, we have systematically studied the catalytic conversion of cellulose to 5-hydroxymethyl furfural using MCM-41 and sulfonated Zr-MCM-41 catalysts in a batch reactor. The characterization results have stated that replacement of Si^{4+} with Zr^{4+} in MCM-41 by in-situ synthesis, the existence of hexagonal mesopores, attachment of sulfate groups to the walls of Zr-MCM-41, and the presence of Bronsted acidic and Lewis acidic sites. The high catalytic conversion of cellulose and selectivity of 5-HMF was obtained for S-15Zr-MCM-41 at 170 °C, for 2 h because of the high ratio of Brønsted acidic to Lewis acidic sites.

Acknowledgements Open access funding provided by University of Szeged. The authors would like to thank the Institute of Chemistry -VAST for funding the project (QTHU 01.01/18-19). This paper was supported by the Hungarian Research Development and Innovation Office through grants NKFIH OTKA PD 120877 of AS and K120115 of KZ. The financial support of the Hungarian National Research, Development, and Innovation Office through the GINOP-2.3.2-15-2016-00013 project "Intelligent materials based on functional surfaces—from syntheses to applications" and the Ministry of Human Capacities through the EFOP-3.6.1-16-2016-00014 and 20391-3/2018/FEKUSTRAT project is also acknowledged.

References

1. Tang Z, Su J (2019) Direct conversion of cellulose to 5-hydroxymethylfurfural (HMF) using an efficient and inexpensive boehmite catalyst. Carbohydr Res 481:52–59
2. Van Putten RJ, Van der Waal JC, De Jong E, Rasrendra CB, Heeres HJ, De Vries JG (2013) Hydroxymethylfurfural, a versatile platform chemical made from renewable resources. Chem Rev 113:1499–1597
3. Bozell JJ, Petersen GR (2010) Technology development for the production of biobased products from biorefinery carbohydrates—the US Department of Energy's "Top 10" revisited. Green Chem 12:539–554
4. De Jong E, Dam MA, Sipos L, Gruter GJM. (2012). Furandicarboxylic acid (FDCA), a versatile building block for a very interesting class of polyesters. ACS Symp Ser, 1–13
5. Zhong S, Daniel R, Xu H, Zhang J, Turner D, Wyszynski ML, Richards P (2010) Combustion and emissions of 2,5-dimethylfuran in a direct-injection spark-ignition engine. Energ Fuel 24:2891–2899
6. Osatiashtiani A, Lee AF, Brown DR, Melero JA, Morales G, Wilson K (2014) Bifunctional SO_4/ZrO_2 catalysts for 5-hydroxymethylfurfural (5-HMF) production from glucose. Catal Sci Technol 4:333–342

7. Yang Y, Hu CW, Abu-Omar MM (2012) Conversion of carbohydrates and lignocellulosic biomass into 5-hydroxymethylfurfural using $AlCl_3{\cdot}6H_2O$ catalyst in a biphasic solvent system. Green Chem 14:509–513
8. Pagán-Torres YJ, Wang T, Gallo JMR, Shanks BH, Dumesic JA (2012) Production of 5- hydroxymethylfurfural from glucose using a combination of lewis and brønsted acid catalysts in water in a biphasic reactor with an alkylphenol solvent. ACS Catal 2:930–934
9. Zhao H, Holladay JE, Brown H, Zhang ZC (2007) Metal chlorides in ionic liquid solvents convert sugars to 5-hydroxymethylfurfural. Sci 316:1597
10. Chan JYG, Zhang Y (2009) Selective conversion of fructose to 5-hydroxymethylfurfural catalyzed by tungsten salts at low temperatures. Chemsuschem 2:731–734
11. Hu S, Zhang Z, Song J, Zhou Y, Han B (2009) Efficient conversion of glucose into 5- hydroxymethylfurfural catalyzed by a common Lewis acid $SnCl_4$ in an ionic liquid. Green Chem 11:1746–1749
12. Li W, Xu Z, Zhang T, Li G, Jameel H, Chang HM, Ma L (2016) catalytic conversion of biomass-derived carbohydrates into 5-hydroxymethylfurfural using a strong solid acid catalyst in aqueous γ-valerolactone. BioRes 11:5839–5853
13. Eminov S, Filippousi P, Brandt A, Wilton-Ely J, Hallett J (2016) Direct catalytic conversion of cellulose to 5-hydroxymethylfurfural using ionic liquids. Inorganics 4:32–46
14. Bhaumik A, Bhanja P (2015) Biomass to bioenergy over porous nanomaterials: a green technology. Trends Green Chem 1:1–8
15. Menegazzo F, Ghedini E, Signoretto M (2018) 5-Hydroxymethylfurfural (HMF) production from real biomasses. Mol 23:2201–2218
16. Wilson K, Lee AF (2016) Catalyst design for biorefining. Philos Trans R Soc A 374:20150081
17. Hara M, Nakajima K, Kamata K (2015) Recent progress in the development of solid catalysts for biomass conversion into high value-added chemicals. Sci Technol Adv Mater 16:034903–034903
18. Mazzotta MG, Gupta D, Saha B, Patra AK, Bhaumik A, Abu-Omar MM (2014) Efficient solid acid catalyst containing lewis and brønsted acid sites for the production of furfurals. Chemsuschem 7:2342–2350
19. Osatiashtiani A, Lee AF, Granollers M, Brown DR, Olivi L, Morales G, Melero JA, Wilson K (2015) Hydrothermally stable, conformal, sulfated zirconia monolayer catalysts for glucose conversion to 5-HMF. ACS Catal 5:4345–4352
20. Sakwa-Novak MA, Holewinski A, Hoyt CB, Yoo CJ, Chai SH, Dai S, Jones CW (2015) Probing the role of Zr addition versus textural properties in enhancement of CO_2 adsorption performance in silica/PEI composite sorbents. Langmuir 31:9356–9365
21. Ogino I, Suzuki Y, Mukai SR (2015) Tuning the pore structure and surface properties of carbon-based acid catalysts for liquid-phase reactions. ACS Catal 5:4951–4958
22. Seelandt B, Wark M (2012) Electrodeposited prussian blue in mesoporous TiO_2 as electrochromic hybrid material. Micropor Mesopor Mat 164:67–70
23. Chen LF, Wang JA, Noreña LE, Aguilar J, Navarrete J, Salas P, Montoya JA, Del Ángel P (2007) Synthesis and physicochemical properties of Zr-MCM-41 mesoporous molecular sieves and Pt/$H_3PW_{12}O_{40}$/Zr-MCM-41 catalysts. J Solid State Chem 180:2958–2972
24. Dehghani S, Haghighi M (2017) Sono-sulfated zirconia nanocatalyst supported on MCM-41 for biodiesel production from sunflower oil: Influence of ultrasound irradiation power on catalytic properties and performance. Ultrason Sonochem 35:142–151
25. Abdel Salam MS, Betiha MA, Shaban SA, Elsabagh AM, Abd El-Aal RM, El kady FY, (2015) Synthesis and characterization of MCM-41-supported nano zirconia catalysts. Egypt J Pet 24:49–57
26. Wróblewska A, Miądlicki P, Tołpa J, Sreńscek-Nazzal J, Koren ZC, Michalkiewicz B (2019) Influence of the Titanium Content in the Ti-MCM-41 Catalyst on the Course of the α-Pinene Isomerization Process. Catalysts 9:396–411
27. Brunauer S, Emmett PH, Teller E (1938) Adsorption of gases in multimolecular layers. J Am Chem Soc 60:309–319
28. Derylo-Marczewska A, Gac W, Popivnyak N, Zukocinski G, Pasieczna S (2006) The influence of preparation method on the structure and redox properties of mesoporous Mn-MCM-41 materials. Catal Today 114:293–306
29. Selvaraj M, Sinha PK, Pandurangan A (2004) Synthesis of dypnone using SO_4^{2-}/Al-MCM-41 mesoporous molecular sieves. Micropor Mesopor Mater 70:81–91
30. Sápi A, Kashaboina U, Ábrahámné KB, Gómez-Pérez JF, Szenti I, Halasi G, Kiss J, Nagy B, Varga T, Kukovecz A, Kónya Z (2019) Synergetic of Pt nanoparticles and H-ZSM-5 zeolites for efficient CO_2 activation: role of interfacial sites in high activity. Front Mater 6:1–12

31. Palai YN, Shrotri A, Asakawa M, Fukuoka A. (2020). Silica supported Sn catalysts with tetrahedral Sn sites for selective isomerization of glucose to fructose. Catal Today